

Glassy dynamics and domains: exact results for the East model

Ramses van Zon

*The Rockefeller University, 1230 York Avenue, New York, New York 10021, USA and
Chemical Physics Theory Group, Dept. of Chemistry,
University of Toronto, Ontario, Canada M5S 3H6*

Jeremy Schofield

*Chemical Physics Theory Group, Dept. of Chemistry,
University of Toronto, Ontario, Canada M5S 3H6*

(Dated: December 8, 2004)

A general matrix-based scheme for analyzing the long-time dynamics in kinetically constrained models such as the East model is presented. The treatment developed here is motivated by the expectation that slowly-relaxing spin domains of arbitrary size govern the highly cooperative events that lead to spin relaxation at long times. To account for the role of large spin domains in the dynamics, a complete basis expressed in terms of domains of all sizes is introduced. It is first demonstrated that accounting for single domains of all possible sizes leads to a simple analytical result for the two-time single-spin correlation function in the East model that is in excellent quantitative agreement with simulation data for equilibrium spin up density values $c \geq 0.6$. It is then shown that including also two neighboring domains leads to a closed expression that describes the slow relaxation of the system down to $c \approx 0.3$. Ingredients of generalizing the method to lower values of c are also provided, as well as to other models. The main advantage of this approach is that it gives explicit analytical results and that it requires neither an arbitrary closure for the memory kernel nor the construction of an irreducible memory kernel. It also allows one to calculate quantities that measure heterogeneity in the same framework, as is illustrated on the neighbor-pair correlation function and the distribution of relaxation times.

PACS numbers: 64.70.Pf, 61.20.Lc, 52.35.Mw, 02.50.Ey

I. INTRODUCTION

Despite much progress in recent years, many aspects of structural glasses and undercooled liquids still escape a complete understanding^{1,2,3,4}. Rather than studying the behavior of molecular glasses, one often investigates the behavior of simple models in the hope to capture the basic physics of such systems. The so-called East model is one of these simple models⁵. It is a classic Ising model with a trivial Hamiltonian in which the stochastic dynamics governing the change of spin leads to a complicated and highly-cooperative evolution of the system. In the East model, any spin has finite probability to flip from up to down or vice-versa only if the spin to the east of it (i.e., of higher lattice index) is up. Models of this kind are generally called kinetically constrained models or facilitating spin models^{6,7,8,9,10}.

Such models are designed to mimic^{10,11,12,13} the kind of dynamics that take place in glasses⁴. Although the East model itself does not have a glass transition at any finite spin density⁵, the decay of the single spin time-correlation function at low densities is a stretched exponential^{7,14}, following a functional form similar to that of the dynamic structure factor in glassy systems^{15,16,17}. In fact, the typical spin relaxation time has been shown to behave as $\log(\tau) \sim \log^2(1/c)$, where c is the equilibrium density of up-spins, heuristically by Sollich and Evans¹⁸ and rigorously by Aldous and Diaconis¹⁹, indicating an extreme slowing down for small c , suggestive of a transition at $c = 0$. More recently, the

East model has been analyzed to examine the nature of dynamic heterogeneities^{11,12} in frustrated systems.

The typical relaxation times present in systems exhibiting frustration can be retrieved from time correlation functions. In glasses, mode coupling theory is one of the predominant descriptions for these correlation functions. Several approaches to mode coupling theories exist. In the context of glasses, that of Götze and co-workers has been widely used^{16,20,21,22,23,24,25,26,27,28,29,30}.

The approach of Götze and co-workers expresses the time correlation functions in terms of a memory kernel and then uses a certain ansatz in which the memory function is written in terms of the correlation functions themselves, yielding self-consistent equations. Oppenheim and co-workers have addressed the formal points and justification of mode coupling theories in Fourier space^{31,32,33,34}. Along similar lines, Andersen³⁵ has formulated a phase-space mode coupling theory for general fluids that leads to self-consistent equations for time dependent correlation functions.

Mode coupling theory can be applied for both deterministic and stochastic systems. For some systems, such as the East model, the application of the most commonly used mode-coupling ansatz necessary to close the resulting equation of motion for the spin autocorrelation function leads to a spurious transition from an ergodic to non-ergodic phase at finite values of the spin concentration c , a result that is clearly at odds with simulation results. To analyze the failure of the closure approximation in

mode coupling theory, Pitts *et al.* have presented a diagrammatic treatment that yields similar equations to those of mode coupling theories of the glass transition⁹. This treatment lends itself to a closure assumption that is very similar kind to the mode coupling theory of Götze *et al.* Pitts *et al.* propose alternative closure assumptions to this mode coupling theory by summing subsets of diagrams. The resulting predictions are in good agreement with simulations for high concentration of up-spins, but still decay too rapidly at lower spin density. Recent improvements on this scheme have been carried out by Wu and Cao¹⁴ based on a combination of matrix methods and mode coupling closure assumptions.

Regardless of the precise formalism, mode coupling theories aim to describe slow long time behavior, and so should include all the “slow modes” of the system. For hydrodynamics of a simple fluid at moderate densities, these slow modes are well-known, namely the density, momentum and energy modes at large wave lengths. Correspondingly, when applied to Fourier modes of these hydrodynamical fields, mode coupling theory (e.g. in the formulation of Oppenheim and co-workers) yields well defined perturbative results when the correlation length is finite and the thermodynamic limit is taken. However, in the case of the East model, the relevant slow modes are less obvious, and previously developed mode coupling theories for this model^{5,8,9,14,36} may have missed some of these slow modes. In fact the absence of some slow modes provides a possible explanation for the problem these theories have with describing the long time behavior at small c .

The main purpose of this article is to identify the relevant slow modes in frustrated spin systems and to describe the impact of the coupling of these modes to a specific spin variable. It is demonstrated that the existence of slowly-relaxing spin domains of arbitrary size suggests a natural basis of slow modes in which quantitatively accurate but simple approximation schemes are easily formulated for many quantities of interest in the study of slow heterogeneous relaxation.

II. THE EAST MODEL

The East model⁵ is a linear chain of N spins, which are numbered from 0 to $N - 1$, with each spin allowed to assume one of two values at any given time, here taken to be up or down. Occupation numbers n_i are defined such that $n_i = 1$ when spin i is up and 0 if it is down. The static properties of this model follow from the Hamiltonian

$$H = \mu \sum_{i=0}^{N-1} n_i. \quad (1)$$

Using the canonical distribution $\rho \sim \exp[-\beta H]$, the average occupation per site if the system is at equilibrium

at an inverse temperature β , is found to be

$$c = 1/(1 + e^{\beta\mu}). \quad (2)$$

As $\beta\mu$ has little physical significance in the current context, the density c will be used as a parameter. If \mathbf{n} denotes a spin state (i.e., a configuration of the N spins), the canonical equilibrium distribution can be written as

$$\rho(\mathbf{n}) = \prod_{i=0}^{N-1} [c n_i + (1 - c)(1 - n_i)] \quad (3)$$

where Eqs. (1) and (2) were used, as well as the fact that n_i is either zero or one. Note that each spin i has a probability c to be up ($n_i = 1$) and $1 - c$ to be down ($n_i = 0$).

For the dynamics, consider the conditional probability density $U_t(\mathbf{n}, \mathbf{n}')$ to be in state \mathbf{n} at time t given that the system was in state \mathbf{n}' at time 0, which satisfies^{9,37}

$$\begin{aligned} \dot{U}_t(\mathbf{n}, \mathbf{n}') &= \sum_{\tilde{\mathbf{n}}} [W(\mathbf{n}, \tilde{\mathbf{n}})U_t(\tilde{\mathbf{n}}, \mathbf{n}') - W(\tilde{\mathbf{n}}, \mathbf{n})U_t(\mathbf{n}, \mathbf{n}')] \\ &\equiv \sum_{\tilde{\mathbf{n}}} \mathcal{L}(\tilde{\mathbf{n}}, \mathbf{n})U_t(\tilde{\mathbf{n}}, \mathbf{n}'), \end{aligned} \quad (4)$$

with $U_0(\mathbf{n}, \mathbf{n}') = \delta_{\mathbf{n}\mathbf{n}'}$. Here, $W(\mathbf{n}, \mathbf{n}')dt$ is the probability to make a transition from \mathbf{n}' to \mathbf{n} in a time dt . By definition, $W(\mathbf{n}, \mathbf{n}) = 0$. Defining

$$A(\mathbf{n}, t) = \sum_{\mathbf{n}'} A(\mathbf{n}')U_t(\mathbf{n}', \mathbf{n}), \quad (5)$$

from Eq. (4) it follows that

$$\dot{A}(\mathbf{n}, t) = \sum_{\mathbf{n}'} \mathcal{L}(\mathbf{n}, \mathbf{n}')A(\mathbf{n}', t).$$

or

$$\dot{A}(t) = \mathcal{L}A(t) \quad (6)$$

where the Liouville operator \mathcal{L} is a linear operator on the 2^N dimensional Hilbert space of functions of \mathbf{n} . The formal solution of Eq. (6) is $A(t) = e^{\mathcal{L}t}A(0)$.

For the East model, $W(\mathbf{n}, \mathbf{n}')$ can be written as a sum over possible moves, i.e., spin flips of individual sites i :

$$W(\mathbf{n}, \mathbf{n}') = \sum_{i=0}^{N-1} W_i(\mathbf{n}, \mathbf{n}').$$

A flip of spin n_i is possible only if $n_{i+1} = 1$ (using the boundary condition that $n_N = 1$), as the expression for W_i bears out⁹:

$$W_i(\mathbf{n}, \mathbf{n}') = [c\delta_{n_i 1}\delta_{n'_i 0} + (1 - c)\delta_{n_i 0}\delta_{n'_i 1}] n_{i+1} \prod_{j \neq i} \delta_{n_j n'_j}.$$

Correspondingly, the Liouville operator can be written as

$$\begin{aligned} \mathcal{L}(\mathbf{n}, \mathbf{n}') &= \sum_{i=0}^{N-1} \left[(1 - c)\delta_{n_i 1} (\delta_{n'_i 0} - \delta_{n'_i n_i}) \right. \\ &\quad \left. + c\delta_{n_i 0} (\delta_{n'_i 1} - \delta_{n'_i n_i}) \right] n_{i+1} \prod_{j \neq i} \delta_{n_j n'_j}. \end{aligned} \quad (7)$$

The equilibrium distribution in Eq. (3) will serve as a weight for the inner product on the Hilbert space, i.e., the inner product of $A(\mathbf{n})$ and $B(\mathbf{n})$ is $\langle A|B\rangle = \sum_{\mathbf{n}} \rho(\mathbf{n})A(\mathbf{n})B(\mathbf{n}) \equiv \langle AB\rangle$. Only real quantities will be used in this paper, so there is no need to define a complex inner product (although this is straightforward). The time correlation function of A and B can now be written as $\langle A(t)|B\rangle$. When $W(\mathbf{n}, \mathbf{n}')\rho(\mathbf{n}') = W(\mathbf{n}', \mathbf{n})\rho(\mathbf{n})$, i.e., when detailed balance holds, as it does in this model, \mathcal{L} is Hermitian with respect to the inner product. In contrast to stochastic systems, in deterministic systems the Liouville operator is anti-Hermitian. It should be noted that the condition of detailed balance also guarantees that the limiting stationary distribution of the Markovian dynamics is the equilibrium distribution (3), provided the underlying Markov process is ergodic³⁷.

As remarked by Pitts et al.⁸, different sites are not only *statically* independent [cf. Eq. (1)], but also *dynamically*. To see this, consider the normalized single site fluctuation

$$\hat{n}_i(t) = \frac{n_i(t) - c}{\sqrt{c(1-c)}}. \quad (8)$$

which satisfies $\langle \hat{n}_i^2(t) \rangle = 1$ and $\langle \hat{n}_i(t) \rangle = 0$. Note that

$$\begin{aligned} \mathcal{L}\hat{n}_i &= -n_{i+1}\hat{n}_i & (9) \\ &= -c\hat{n}_i + \sqrt{c(1-c)}\hat{n}_i\hat{n}_{i+1}, & (10) \end{aligned}$$

using Eqs. (7) and (8). Thus, the time derivative of \hat{n}_i depends on the product of \hat{n}_i and \hat{n}_{i+1} . The derivative of that product will in turn depend on \hat{n}_{i+2} , and so on. Thus, $\hat{n}_{i'}(t) = e^{\mathcal{L}t}\hat{n}_{i'}$ involves only \hat{n}_i with $i \geq i'$. From the static independence of any site i and any other site i'' with $i'' < i' \leq i$, it follows that $\langle \hat{n}_{i'}\hat{n}_{i'}(t) \rangle = \langle \hat{n}_{i'} \rangle \langle \hat{n}_{i'}(t) \rangle = 0$. Because \mathcal{L} is Hermitian, also $\langle \hat{n}_{i''}(t)\hat{n}_{i'} \rangle = 0$. So all time correlation functions between different sites $i' \neq i''$ are zero.

Given the dynamical independence of different sites, we are interested in the nontrivial time correlation function

$$C(t) = \langle \hat{n}_i(t)\hat{n}_i(0) \rangle. \quad (11)$$

In the limit $N \rightarrow \infty$ with i fixed, this is independent of i due to translation invariance. This single spin time correlation function in the thermodynamic limit is the main quantity of interest.

III. PROJECTION OPERATOR TECHNIQUES

In a mode coupling framework, dynamical equations are derived for the time correlation functions of slow modes in the system, which involves a memory kernel that is again expressed in terms of the correlation functions^{8,38,39}. The starting point is often a projection operator formalism. Here, a general setup will be presented, which uses the Mori-Zwanzig projection operator formalism^{39,40}, to be specialized later.

Let A_k be the slow modes of the system determined from physical arguments, with k an index running over the slow modes. It will be assumed that $\langle A_k \rangle = 0$ (as could be achieved by subtracting the average), and that A_k are orthonormal, i.e., $\langle A_k|A_q \rangle = \delta_{kq}$ (as could be achieved by a Gram-Schmidt procedure). For brevity, the A_k 's are taken together in a vector A . In the projection operator formalism, the component along A of any other physical quantity B is found using the projection operator

$$\mathcal{P}B = \langle B|A \rangle \cdot A = \sum_k \langle B|A_k \rangle A_k, \quad (12)$$

where \cdot denotes a vector product, i.e., a sum over k , as indicated. Using the operator identity

$$e^{\mathcal{L}t} = e^{(1-\mathcal{P})\mathcal{L}t} + \int_0^t e^{\mathcal{L}\tau} \mathcal{P} \mathcal{L} e^{(1-\mathcal{P})\mathcal{L}(t-\tau)} d\tau, \quad (13)$$

and Eqs. (6) and (12), one can derive that

$$\dot{A}(t) = \mathbf{M}^E \cdot A(t) + \int_0^t \mathbf{M}^D(t-\tau) \cdot A(\tau) d\tau + \varphi(t), \quad (14)$$

where $\varphi(t) = e^{(1-\mathcal{P})\mathcal{L}t}(1-\mathcal{P})\mathcal{L}A$ and

$$\mathbf{M}^E = \langle A|\mathcal{L}|A \rangle \quad (15)$$

$$\mathbf{M}^D(t) = \langle \varphi(t)|\varphi \rangle. \quad (16)$$

Note that \mathbf{M}^E and $\mathbf{M}^D(t)$ are matrices whose dimensions are equal to the number of slow modes and that \mathbf{M}^E contains only static information, while the memory kernel $\mathbf{M}^D(t)$ involves the time correlation of the fluctuating force $\varphi(t)$.

Taking the inner product with A , Eq. (14) yields an equation for the correlation function $\mathbf{G}(t) \equiv \langle A(t)|A \rangle$:

$$\dot{\mathbf{G}}(t) = \mathbf{M}^E \cdot \mathbf{G}(t) + \int_0^t \mathbf{M}^D(t-\tau) \cdot \mathbf{G}(\tau) d\tau. \quad (17)$$

To solve this equation, a Laplace transform will be used, defined as

$$\tilde{\mathbf{G}}(z) = \int_0^\infty e^{-zt} \mathbf{G}(t) dt. \quad (18)$$

Here and the following, we adopt the convention that quantities with a tilde ($\tilde{}$) are z -dependent. The solution in Laplace space of Eq. (17) is

$$\tilde{\mathbf{G}} = (z\mathbb{1} - \mathbf{M}^E - \tilde{\mathbf{M}}^D)^{-1}. \quad (19)$$

where

$$\tilde{\mathbf{M}}^D = \int_0^\infty e^{-zt} \mathbf{M}^D(t) dt. \quad (20)$$

IV. PHYSICS OF THE SLOW DYNAMICS

If A in the previous section contained all the slow behavior, then $M^D(t)$ would be a quickly-decaying function that could be replaced by a delta function in time and integrated over in Eq. (17)^{38,39}. Unfortunately, this is typically not the case because the projection operator $(1 - \mathcal{P})$ only removes part of the dependence on A . For instance in a fluid, the long wave length modes of density, momentum and energy are slow because they correspond to densities of conserved quantities, but only at low densities is it enough to consider only these modes as slow. Extending the set A by multi-linear modes^{31,41}, can help, and can be used to setup self-consistent equations which are exact in the thermodynamic limit provided there is a finite dynamical correlation length^{31,32,33,34}.

As is known from the extensive work of Götze and co-workers^{16,20,21,22,23,24,25,26,27,28,29,30} in deterministic systems, such self-consistent equations can give rise to a glass transition.

If, on the other hand, A is a complete set, then $1 - \mathcal{P} = 0$ and consequently $\varphi(t) = 0$ and $M^D(t) = 0$. In this case, the above formalism corresponds to writing Eq. (6) in a particular basis. This formulation is often applied to the East model^{8,9,14}. When working with a complete basis set, the set still has to be truncated at some level in practice. This introduces truncations errors, or, viewed alternatively, a nonzero $M^D(t)$. To get beyond the truncation problem, one makes an ansatz for the memory kernel in terms of the time correlation function of interest [here $C(t)$], yielding a self-consistent equation. However, in stochastic systems, a glass transition will not be found if such an ansatz is used for the memory kernel, due to the Hermitian nature of \mathcal{L} ^{9,14}. Rather, an ansatz needs to be used for the so-called “irreducible” memory kernel^{36,42}. Then, a glass transition can be found for finite c in the East model^{8,9}. However, simulations make it clear that there is no transition to a non-ergodic phase at a non-zero value of c . Somewhat better schemes to improve the ansatz have been developed since¹⁴, but generally, they lead either to a transition or to a time correlation function that decays too quickly.

Essential for the success of mode coupling theories for fluids at lower densities is the finiteness of the dynamical correlation length, which gives a cutoff length and certain exact factorization properties in the thermodynamic limit^{31,32}. However, for the East model, no such length scale exists, as is seen when one contrasts the result of the scaling of the decay time^{18,19} vs. the diagrammatic approach of Pitts and Anderson⁹. When diagrams are truncated at a certain level, corresponding to taking into account only spins within a certain distance l , the memory kernel becomes a polynomial in c of which highest power is c^l , which means the typical time can scale at the slowest as c^{-l} . However, for $c \rightarrow 0$, the timescale diverges faster than any inverse power of c ^{18,19}. So clearly the spins at all positions, arbitrarily far away, need to be taken into account.

A second way to see that the dynamic correlation length is unbounded is to note that while the static correlation length is zero, dynamically, the decay of the time correlation function $C(t)$ is influenced by other spins. For example, if there is a large domain of down spins to the east of a given spin, that particular spin requires a long time to flip since all down spins in the domain must flip at least once. Hence, the decay is correlated with the existence of this domain, and the dynamic correlation length is therefore at least of the order of the size of this domain. But domains of all sizes exist and larger sized domains will contribute to the behavior of the time correlation function $C(t)$ at longer times. Even if one is only interested in the bulk of the behavior of the time correlation function $C(t)$, for which the relevant domains are of typical size $1/c$, this size diverges as $c \rightarrow 0$. Therefore, it is no surprise that fixed spatial truncations do not work below a certain value of c and that mode coupling theories using such truncations have problems to describe the long time behavior of the time correlation function $C(t)$. For a different formulation of the importance of domains, see Garrahan and Chandler^{11,12} and Wu and Cao¹⁴.

Thus, physically, the origin of the slowness of the dynamics seems to be related to the absence of a finite dynamical correlation length and the existence of arbitrarily large domains of down spins.

V. THE DOMAIN BASIS

A. Single domains

Consider the leftmost spin n_0 in a semi-infinite chain of spins. East of this leftmost spin (i.e., at sites $i > 0$), a domain of typical size $1/c$ filled with down spins exists. In the previous section it was argued that the presence of these domains is essential to the dynamics, so they should somehow be included. This is achieved by defining the (single) *domain basis*, which is composed of the orthonormal basis vectors

$$\hat{Q}_0 = \frac{1}{Z_0}(n_0 - c) \quad (21)$$

and

$$\hat{Q}_1(0) = \frac{1}{Z_1(0)}(n_0 - c)(n_1 - c) \quad (22a)$$

$$\hat{Q}_1(1) = \frac{1}{Z_1(1)}(n_0 - c)(1 - n_1)(n_2 - c) \quad (22b)$$

and in general

$$\hat{Q}_1(k) = \frac{1}{Z_1(k)}(n_0 - c) \prod_{j=1}^k (1 - n_j)(n_{k+1} - c). \quad (22c)$$

where the normalization constants are to be chosen such that $\langle \hat{Q}_0^2 \rangle = \langle [\hat{Q}_1(k)]^2 \rangle = 1$. Note that in Eqs. (22) each factor $(1 - n_j)$ only yields a contribution when $n_j = 0$,

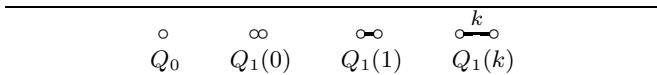


TABLE I: Diagrammatic representation of the domain basis.

i.e., when spin j is down. Thus, a consecutive sequence of such factors represents a down-spin domain.

Comparing the basis vector in Eq. (21) to \hat{n}_0 in Eq. (8), which is normalized, it is seen that \hat{Q}_0 should be equal to \hat{n}_0 , *i.e.*,

$$Z_0 = \sqrt{c(1-c)}. \quad (23)$$

Using a convenient diagrammatic representation we will later derive that

$$Z_1(k) = c(1-c)^{1+k/2}. \quad (24)$$

Other useful quantities will be the unnormalized versions of these basis vectors

$$Q_0 = (n_0 - c) \quad (25)$$

$$Q_1(k) = (n_0 - c) \prod_{j=1}^k (1 - n_j)(n_{k+1} - c). \quad (26)$$

Note that

$$\hat{Q}_0 = Q_0/Z_0 \quad (27a)$$

$$\hat{Q}_1(k) = Q_1(k)/Z_1(k). \quad (27b)$$

It is convenient at this point to introduce a diagrammatic notation for the unnormalized quantities Q_0 and Q_1 , depicted in Table I. In such diagrams, the horizontal direction represents the lattice. An open circle (\circ) at a certain position i denotes $(n_i - c)$, a horizontal line (---) denotes $(1 - n_i)$ and a product of consecutive $(1 - n_i)$'s is represented as a longer horizontal line with the number of factors written on top of the line. When these diagrammatic elements are touching, this denotes that they are on neighboring lattice sites. The first (*i.e.*, leftmost) symbol in a diagram will always refer to site 0. Note that after a diagram for Q_0 and Q_1 has been evaluated, one still has to divide by the appropriate normalization to get the quantities corresponding to \hat{Q}_0 and \hat{Q}_1 , *cf.* Eqs. (27).

As an example, this diagrammatic notation will be used to show that Eq. (24) is the correct choice for $Z_1(k)$ such that $\langle \hat{Q}_1(k') | \hat{Q}_1(k) \rangle$ is equal to $\delta_{kk'}$. The product of $Q_1(k)$ and $Q_1(k')$ will be represented as the two diagrams of $Q_1(k)$ and $Q_1(k')$ from Table I on top of each other:

$$\langle Q_1(k') | Q_1(k) \rangle = \langle \overset{k'}{\circ} \text{---} \circ | \overset{k}{\text{---}} \circ \rangle = \frac{k}{k'} \frac{\circ}{\circ} \quad (28)$$

The vertical displacement of the two parts in the diagram on the right hand side serves to distinguish one part from the other and to indicate that the diagram needs to be averaged. Next, note that since $\langle \circ \rangle = \langle n_i - c \rangle = 0$, any

open circle at site i in the diagram has to overlap with an open circle or a horizontal line at the same site i from the other part in order to give a non-vanishing contribution to the average. In the diagram in Eq. (28), this can only happen if $k = k'$. Thus, the domain basis is orthogonal. The case $k = k'$ is represented by

$$\langle Q_1(k) | Q_1(k) \rangle = \frac{k}{k} \frac{\circ}{\circ} = c^2(1-c)^{k+2}. \quad (29)$$

In the last equality, we used that different parts of a diagram have different contributions depending on which diagrammatic elements on top align with which elements on the bottom, as shown in Table II (the diagrammatic element “ \bullet ” will be introduced later). The contributions of the various parts are simply multiplied because each site is (statically) independent. From Eqs. (27b) and (29) it follows that

$$\langle \hat{Q}_1(k) | \hat{Q}_1(k) \rangle = \frac{\langle Q_1(k) | Q_1(k) \rangle}{[Z_1(k)]^2} = \frac{c^2(1-c)^{k+2}}{[Z_1(k)]^2}. \quad (30)$$

With the definition of $Z_1(k)$, Eq. (24), we immediately see that the $\hat{Q}_1(k)$ are properly normalized. In a similar way, one can deduce that $\langle \hat{Q}_0 | \hat{Q}_1(k) \rangle = 0$, thus establishing that the basis is really orthonormal.

Taking the collection $\{\hat{Q}_0, \hat{Q}_1\}$ for A in the projection formalism of Sec. III, the matrix M^E in Eq. (15) which determines the dynamics, becomes

$$M^E = \begin{bmatrix} \langle \hat{Q}_0 | \mathcal{L} | \hat{Q}_0 \rangle & \langle \hat{Q}_0 | \mathcal{L} | \hat{Q}_1 \rangle \\ \langle \hat{Q}_1 | \mathcal{L} | \hat{Q}_0 \rangle & \langle \hat{Q}_1 | \mathcal{L} | \hat{Q}_1 \rangle \end{bmatrix}, \quad (31)$$

where \hat{Q}_1 without a value of k denotes the column vector (in the ket) or row vector (in the bra) composed of all $\hat{Q}_1(k)$. From Eqs. (7) and (9) it follows that

$$\mathcal{L}Q_0 = -(n_0 - c)n_1 = -\infty \quad (32a)$$

$$\begin{aligned} \mathcal{L}Q_1(0) &= -(n_0 - c)[(n_1 - c)n_2 + n_1(1 - c)] \\ &= -\infty \bullet - (1 - c) \bullet \end{aligned} \quad (32b)$$

$$\begin{aligned} \mathcal{L}Q_1(k \geq 1) &= (n_0 - c)(1 - n_1) \cdots (1 - n_{k-1}) \\ &\quad \times [-(1 - n_k)(n_{k+1} - c)n_{k+2} \\ &\quad \quad + (n_k - c)n_{k+1}(1 - c)] \\ &= -\overset{k}{\text{---}} \bullet + (1 - c) \overset{k-1}{\text{---}} \bullet \end{aligned} \quad (32c)$$

In the diagrammatic representation in Eqs. (32a)–(32c), a solid circle \bullet denotes n_{k+1} or n_{k+2} .

A few words are in order on how to obtain the diagram of $\mathcal{L}X$ given that of X . The Liouville operator \mathcal{L} acts much like a differential operator and can be shown to follow the product rule $\mathcal{L}(AB) = A(\mathcal{L}B) + (\mathcal{L}A)B$, provided A and B do not involve the same site. Thus, \mathcal{L} acting on diagrams like those in Table I yields a sum of terms where \mathcal{L} acts on each site individually. Each site has one of the diagrammatic elements \circ , \bullet or --- , and

$$\mathcal{L}\circ = -\bullet, \quad \mathcal{L}\bullet = -\circ, \quad \mathcal{L}\text{---} = \bullet. \quad (33)$$

element:	○	-	●	(nothing)		
meaning:	$n - c$	$1 - n$	n	1		
when averaged, results in:	0	$1 - c$	c	1		
horizontal part:	≡	⊗	⊙	⊚	⊗	⊙
meaning:	$(1 - n)^2$	$n(n - c)$	$n(1 - n)$	n^2	$(n - c)^2$	$(1 - n)(n - c)$
when averaged, results in:	$(1 - c)$	$c(1 - c)$	0	c	$c(1 - c)$	$-c(1 - c)$

TABLE II: Rules for the contributions to a diagram. On top are the elementary diagrammatic elements, at the bottom combinations of them. The resulting factors are obtained using Eq. (3).

Thus, \mathcal{L} acting on site i introduces a new diagrammatic element \bullet in the diagram on the next site $i + 1$. If the diagram already had an element on that site, one needs to multiply the new one with the original one, and this gives the three possibilities

$$\bullet \times \circ = (1 - c)\bullet, \quad \bullet \times \bullet = \bullet, \quad \bullet \times - = 0. \quad (34)$$

As the last equation shows, \mathcal{L} acting on an element at site i yields zero if site $i + 1$ has the diagrammatic element “-”. This is the reason why there are so few diagrams in Eqs. (32c): although \mathcal{L} could in principle act on all sites in $Q_1(k)$, most have an element “-” to their right and yield zero.

The matrix elements $\langle Q_0 | \mathcal{L} | Q_0 \rangle$, $\langle Q_0 | \mathcal{L} | Q_1(k) \rangle$ and $\langle Q_1(k') | \mathcal{L} | Q_1(k) \rangle$ are found by taking the inner product of the diagrams in Eq. (32) with those of Q_0 and $Q_1(k')$ in Table I. Because each open circle needs to be covered, the only nonzero contributions are for $k' = k - 1, k$ and $k + 1$, and

$$\langle Q_0 | \mathcal{L} | Q_0 \rangle = -8\bullet = -c^2(1 - c) \quad (35a)$$

$$\langle Q_1(0) | \mathcal{L} | Q_0 \rangle = -8\bullet = -c^2(1 - c)^2 \quad (35b)$$

$$\begin{aligned} \langle Q_1(0) | \mathcal{L} | Q_1(0) \rangle &= -8\bullet\bullet - (1 - c)8\bullet \\ &= -c^2(1 - c)^2 \end{aligned} \quad (35c)$$

$$\begin{aligned} \langle Q_1(k) | \mathcal{L} | Q_1(k) \rangle &= -8\overset{k}{\bullet\bullet} + (1 - c)\overset{k-1}{\bullet\bullet} \\ &= -c^3(2 - c)(1 - c)^{k+2} \text{ if } k > 0 \end{aligned} \quad (35d)$$

and

$$\langle Q_1(k + 1) | \mathcal{L} | Q_1(k) \rangle = -8\overset{k}{\bullet\bullet} = c^3(1 - c)^{k+3}, \quad (35e)$$

where the rules in Table II were used. Using Eqs. (27), (31) and (35), M^E becomes the infinite tridiagonal matrix

$$M^E = \begin{bmatrix} -c & -\sqrt{c(1 - c)} & & & \\ -\sqrt{c(1 - c)} & -1 & c\sqrt{1 - c} & & \\ & c\sqrt{1 - c} & -c(2 - c) & \ddots & \\ & & \ddots & \ddots & \ddots \end{bmatrix}, \quad (36)$$

where diagonal dots denote repetition of the last mentioned expression on that diagonal.

At this stage, $M^D(t)$ in Eq. (17) and \tilde{M}^D in Eq. (19) will be set to zero. The reasons for this are twofold. First, it allows an exact solution for spin autocorrelation functions to be obtained that is in good quantitative agreement with simulations if the density of up-spins c is not too low. Secondly, we will later complete the basis such that \tilde{M}^D is in fact strictly zero. Eq. (19) yields in this approximation:

$$\tilde{G} \approx \tilde{G}^{(1)} \equiv (z\mathbb{1} - M^E)^{-1}. \quad (37)$$

Here, the superscript (1) indicates that the result is only a first approximation. Below we will make this into a systematic approximation scheme in which further, more accurate approximations can be obtained.

According to Eq. (21), the Laplace transform of the correlation $C(t)$ in Eq. (11) is the top left element of the matrix \tilde{G} ,

$$\tilde{C} = \int_0^\infty dt e^{-zt} C(t) = \tilde{G}_{11}. \quad (38)$$

To perform the matrix inversion in Eq. (37), one uses the fact that the inverse of a tridiagonal matrix can be performed exactly. In particular, the top left element of the inverse of a symmetric tridiagonal matrix can be

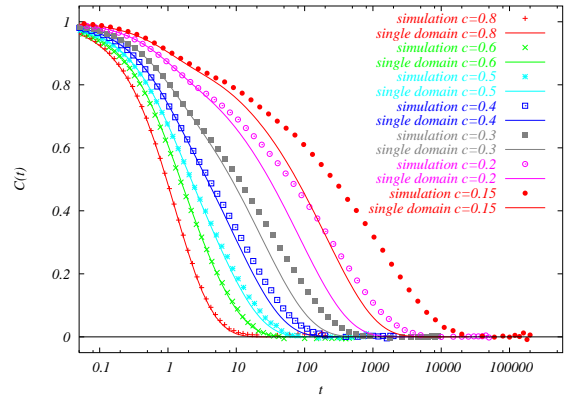


FIG. 1: Results for the single spin time correlation function $C(t)$ from the single domain basis $\{Q_0, Q_1\}$ [by numerical Laplace inversion of Eq. (44) in Sec. V A using *Mathematica*], compared to simulation data (kindly provided by Prof. H. C. Anderson).

written as a continued fraction:

$$\left[\begin{array}{ccc} a_1 & b_1 & \\ b_1 & a_2 & b_2 \\ & b_2 & a_3 \quad \ddots \\ & & \ddots \quad \ddots \end{array} \right]_{11}^{-1} = \frac{1}{a_1 - \frac{b_1^2}{a_2 - \frac{b_2^2}{a_3 - \dots}}} \quad (39)$$

Combining Eq. (36)–(39), one finds

$$\begin{aligned} \tilde{C}^{(1)} &= \left[\begin{array}{ccc} z+c & \sqrt{c(1-c)} & \\ \sqrt{c(1-c)} & z+1 & -c\sqrt{1-c} \\ & -c\sqrt{1-c} & z+c(2-c) \quad \ddots \\ & & \ddots \quad \ddots \end{array} \right]_{11}^{-1} \\ &= \frac{1}{z+c - \frac{c(1-c)}{z+1 - \frac{c^2(1-c)}{z+c(2-c) - \frac{c^2(1-c)}{z+c(2-c)-\dots}}} \quad (40) \end{aligned}$$

The repeating part of this expression is

$$\tilde{\gamma}^{(1)} = \frac{c^2(1-c)}{z+c(2-c) - \frac{c^2(1-c)}{z+c(2-c)-\dots}} \quad (41)$$

This $\tilde{\gamma}^{(1)}$ clearly satisfies

$$\tilde{\gamma}^{(1)} = \frac{c^2(1-c)}{z+c(2-c) - \tilde{\gamma}^{(1)}} \quad (42)$$

which is solved by

$$\tilde{\gamma}^{(1)} = \frac{1}{2} \left\{ z+c(2-c) - \sqrt{4cz + (z-c^2)^2} \right\}. \quad (43)$$

[Note that the solution of Eq. (42) with a plus sign in front of the square root in Eq. (43) does not go as $1/z$ for large z , and is therefore not in agreement with Eq. (41)]. Inserting this result in Eq. (40), one obtains the explicit form

$$\tilde{C}^{(1)} = \frac{1}{z+c - \frac{2c(1-c)}{z+2 - (2-c)c + \sqrt{4cz + (z-c^2)^2}}} \quad (44)$$

The exact correlation function in Eq. (44) can be Laplace inverted numerically using Stehfest's algorithm^{43,44} (for example, in *Mathematica*⁴⁵). For various values of c , the results are shown in Fig. 1 and compared with data from simulations on the East model. Despite the simple form of $\tilde{C}^{(1)}$ in Eq. (44), there is excellent agreement between this theoretical result and the data for $0.6 \leq c \leq 1$, reasonable qualitative agreement up to $c \approx 0.5$, while the predicted decay is clearly too fast for $c < 0.5$.

B. Inclusion of neighboring domains: a complete basis

There is a need to extend the single domain basis because it does not properly capture the long time behavior of $C(t)$ for c less than 0.5, as seen from Fig. 1. The lack of quantitative agreement between theory and simulation at long times implies essentially that there is important slow behavior in the memory function $M^D(t)$ given in Eq. (16) that cannot be neglected.

This situation is reminiscent of that in fluids. There, one starts out describing time correlation functions in terms of the *linear* dependence on the hydrodynamic fields of mass, momentum and energy density, i.e., one takes these to comprise the set A of Sec. III^{38,39}. But at lower temperatures or higher densities this does not suffice because $M^D(t)$ turns out to no longer be a fast decaying function. To fix this situation, i.e., to represent the missed slow behavior in $M^D(t)$, one needs to augment the linear basis by vectors orthogonal to it. For this, one can take products of A (with proper subtractions to assure orthogonality); these additional basis vectors are called *multi-linear modes*^{31,41}. The coupling of the linear modes to the multi-linear ones “renormalizes” the bare values of M^D found using only A to $M^D + \tilde{\Sigma}(z)$, where $\tilde{\Sigma}$ is a *self-energy*. The z dependence of this self-energy is such that it can describe slowly decaying behavior such as long-time tails. Since the multi-linear modes can be interpreted as products of linear hydrodynamics modes, this procedure amounts to a nonlinear coupling of hydrodynamic modes and is hence called mode-coupling theory.

Similarly, if for the East model, the matrix M^E is taken to be represented at the linear level by Eq. (36), where the linear basis (using analogous nomenclature as above) composing the set of slow variables is taken to be $A = \{\hat{Q}_0, \hat{Q}_1\}$, then the memory function corresponds to an infinite square matrix represented at the linear-linear level that effectively renormalizes the matrix elements of M^E to $M^E + \tilde{M}^D$, according to Eq. (19). Hence, \tilde{M}^D takes the role of the self-energy here, and must describe contributions to the decay of the spin-spin correlation function due to the projection of the dynamical evolution onto a space orthogonal to the linear basis set A . In other words, the single domain basis does not span the ergodic component and fails to capture all the slow dynamics of the spin fluctuation variable \hat{Q}_0 . To represent the missed slow evolution, the single domain basis set must be expanded to include additional slow modes and their coupling to the linear modes must be computed.

To deduce the appropriate extension of the basis, it is helpful to realize, as Fig. 1 shows, that the decay of $C(t)$ that is predicted by the extended linear basis, $\{\hat{Q}_0, \hat{Q}_1\}$, is too rapid. A reasonable explanation of this particular deviation is that in the single domain basis, the final spin n_{k+1} in Eq. (22c) decays regardless of the spin configuration to its right. As a result, any slowing down effect of a persistent down-spin domain to the right of n_{k+1} is missed. It therefore seems natural to try to fix the too


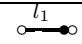
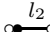
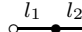
	
$Q_2(0,0) = R(0)$	$Q_2(l_1,0) = R(l_1)$
	
$Q_2(0,l_2) = S(0,l_2-1)$	$Q_2(l_1,l_2) = S(l_1,l_2-1)$

TABLE III: Diagrams of the extension of the domain basis. (The notation using R and S is used only in the appendix.)

rapid decay of the $C(t)$ by augmenting the basis with a second down-spin domain,

$$\hat{Q}_2(l_1, l_2) = \frac{1}{Z_2(l_1, l_2)} (n_0 - c) \prod_{j_1=1}^{l_1} (1 - n_{j_1}) n_{l_1+1} \times \prod_{j_2=l_1+2}^{l_1+l_2+1} (1 - n_{j_2}) (n_{l_1+l_2+2} - c), \quad (45)$$

which carries an index doublet (l_1, l_2) of which each member l_j can take integer values from zero to infinity, and

$$Z_2(l_1, l_2) = c^{3/2} (1 - c)^{1+[l_1+l_2]/2}. \quad (46)$$

As before, unnormalized versions $Q_2(l_1, l_2) = Z_2(l_1, l_2) \hat{Q}_2(l_1, l_2)$ are defined as well:

$$Q_2(l_1, l_2) = (n_0 - c) \prod_{j_1=1}^{l_1} (1 - n_{j_1}) n_{l_1+1} \times \prod_{j_2=l_1+2}^{l_1+l_2+1} (1 - n_{j_2}) (n_{l_1+l_2+2} - c), \quad (47)$$

Diagrammatic representations of the $Q_2(l_1, l_2)$ are shown in Table III. These are orthogonal to Q_0 , as well as to Q_1 , since in a diagrammatic representation of $\langle Q_0 | Q_2(l_1, l_2) \rangle$, the trailing open circle ($n_{l_1+l_2+2} - c$) of Q_2 is not covered, yielding zero, and in the diagram of $\langle Q_1(k) | Q_2(l_1, l_2) \rangle$, it is impossible to line up the trailing open circles of $Q_1(k)$ and $Q_2(l_1, l_2)$ without having the solid dot $\bullet (=n)$ overlap with a horizontal line $- (=1 - n)$, which yields zero [cf. Table II]. It is easy to establish that the $\hat{Q}_2(l_1, l_2)$ are also orthonormal among themselves.

There is no obvious reason to stop this procedure at the two-domain, or “bi-linear”, level and, in fact, the basis can be extended to a complete set in the relevant ergodic component in a straightforward fashion. The elements of this complete basis are most easily written diagrammatically as a sequence of α down-spin domains of different sizes k_j , separated by single up-spins:

$$\hat{Q}_\alpha(k_1, \dots, k_\alpha) = \frac{1}{Z_\alpha(k_1, \dots, k_\alpha)} \circ \overset{k_1}{\bullet} \overset{k_2}{\bullet} \dots \overset{k_\alpha}{\bullet}. \quad (48)$$

Here, $\alpha = 0 \dots \infty$, $k_j = 0 \dots \infty$ ($j = 1 \dots \alpha$) and

$$Z_\alpha(k_1, \dots, k_\alpha) = \begin{cases} c^{1/2} (1 - c)^{1/2} & \text{if } \alpha = 0 \\ c^{(1+\alpha)/2} (1 - c)^{1+\sum_{j=1}^{\alpha} k_j/2} & \text{otherwise.} \end{cases} \quad (49)$$

It is easy to see that the \hat{Q}_α are all independent: the inner product of two of them is zero unless their diagrams [as in Eq. (48)] are equally long, so that both open circles are covered. But then the interior of the diagrams has to have matching top and bottom parts too, otherwise a solid dot and a horizontal line occur at the same site, and this gives zero (Table II). The only nonzero inner product of a $\hat{Q}_\alpha(k_1, \dots, k_\alpha)$ is therefore with itself. Due to our choice of normalization $\langle [\hat{Q}_\alpha(k_1, \dots, k_\alpha)]^2 \rangle = 1$. Since each \hat{Q}_α is orthonormal to all others, each contributes a unique direction in the Hilbert space to the basis which could not be formed from the others: The \hat{Q}_α are independent.

To also establish completeness, we will now count the number of element of the above basis in the finite system of N spins. In that system, there exist only \hat{Q}_α for which $\alpha + 1 + \sum_{j=1}^{\alpha} k_j \leq N$ (which also limits $\alpha < N$). Elementary combinatorics shows that the number of different \hat{Q}_α for given α and N is $\binom{N-1}{\alpha}$. The total number of \hat{Q}_α is thus $\sum_{\alpha}^{N-1} \binom{N-1}{\alpha} = 2^{N-1}$. Thus the above set of 2^{N-1} basis vectors covers only half of the full Hilbert space, which has 2^N dimensions. But it is easy to see which basis vectors are missing and why they are not important. The expression in Eq. (48) always starts with $n_0 - c$, even though the first spin can have two values. Independent vectors can be found by taking a different expression for the first spin. In fact, one can take 1, i.e., one could consider variants of the basis vectors in Eq. (48) in which the factor of $(n_0 - c)$ is not present. Call these \hat{Q}_β , of which there are as many as there are \hat{Q}_α . These new vectors are orthogonal to each other as well as to the \hat{Q}_α because in $\langle \hat{Q}_\alpha | \hat{Q}_\beta \rangle$ the initial \circ in the diagram of \hat{Q}_α is not covered by the diagram of \hat{Q}_β and $\langle \circ \rangle = 0$. Thus, the \hat{Q}_β are the missing basis vectors. However, they are completely unimportant here because the \hat{Q}_β are also orthogonal to $\mathcal{L}\hat{Q}_\alpha$, as is seen from the fact that $\mathcal{L}\hat{Q}_\alpha$ will always have a “ \circ ” as a first element ($\mathcal{L}\circ = -\bullet$) so that the inner product with \hat{Q}_β is zero (for this it is important *not* to have periodic boundary conditions).

So the basis set \hat{Q}_α is not a complete basis for all possible spin configurations, but it *is* a complete orthonormal basis for all spin configurations to which the \hat{Q}_α couple.

These considerations also imply that the East model is not ergodic: the state space contains at least two ergodic components, which are such that a configuration in one of them can never make a transition to any configuration in the other. Noting that the space spanned by \hat{Q}_β contains all quantities insensitive to the value of n_0 , one realizes that it constitutes an East model with an effective length of $N - 1$. The argument above then shows that the state space of this smaller East model can also be split into at least two ergodic components. Applying this argument recursively reveals that there are $N + 1$ ergodic components. The p -th ergodic component consists of functions not sensitive to the values of spins n_0 through some n_{p-1} , with $0 \leq p \leq N$, and has 2^{N-p-1} dimensions if $p < N$ and one dimension if $p = N$. The collection of these ergodic components has $1 + \sum_{p=0}^{N-1} 2^{N-p-1} = 2^N$

dimensions, and thus indeed spans the full Hilbert space of the spin chain of length N .

Since we are interested in the time auto-correlation function of spin n_0 , the relevant ergodic component is the one spanned by \hat{Q}_α , and we conclude that the \hat{Q}_α are the only basis vectors needed. Having established the ‘‘relevant completeness’’, one can take the limit $N \rightarrow \infty$ again, so we need not worry about the boundary condition imposed on n_N .

The extension of the basis set to include an arbitrary number of domains is useful in developing a systematic approach to generate successive improvements for \tilde{C} for lower c . Since the basis $A = \{\hat{Q}_\alpha\}$ spans the ergodic component of \hat{Q}_0 , it follows that $\varphi(t) = e^{(1-\mathcal{P})\mathcal{L}t}(1 - \mathcal{P})\mathcal{L}\hat{Q}_0 = 0$ and the memory function $M^D(t)$ vanishes. Hence, from Eq. (19), $\tilde{G}(z) = (z\mathbb{1} - M)^{-1}$, where the full matrix $M = M^E$ in this complete basis can be written as

$$M = \begin{bmatrix} M_{00} & M_{01} & & & \\ M_{01}^\dagger & M_{11} & M_{12} & & \\ & M_{12}^\dagger & M_{22} & \ddots & \\ & & & \ddots & \ddots \end{bmatrix} \quad (50)$$

where $M_{\alpha\beta} = \langle \hat{Q}_\alpha | \mathcal{L} | \hat{Q}_\beta \rangle$ and it was used that this is zero unless $|\alpha - \beta| < 2$, as can easily be shown (also, diagonal dots do not denote repetition now: all $M_{\alpha\beta}$ can be different). Generalizing Eq. (39) by repeatedly applying the matrix equality (see e.g. Ref.⁴⁶, page 70)

$$\begin{bmatrix} a & c \\ d & b \end{bmatrix}^{-1} = \begin{bmatrix} [a - \frac{cd}{b}]^{-1} & -[a - \frac{cd}{b}]^{-1}cb^{-1} \\ -[b - \frac{dc}{a}]^{-1}da^{-1} & [b - \frac{dc}{a}]^{-1} \end{bmatrix}, \quad (51)$$

one finds

$$\tilde{C}(z) = \begin{bmatrix} z\mathbb{1} - M_{00} & -M_{01} & & & \\ -M_{01} & z\mathbb{1} - M_{11} & -M_{12} & & \\ & -M_{12}^\dagger & z\mathbb{1} - M_{22} & \ddots & \\ & & & \ddots & \ddots \end{bmatrix}_{11}^{-1} \quad (52)$$

$$= \frac{1}{z\mathbb{1} - M_{00} - \frac{M_{01} M_{01}^\dagger}{z\mathbb{1} - M_{11} - \frac{M_{12} M_{12}^\dagger}{z\mathbb{1} - M_{22} - \dots}}} \quad (53)$$

$$= \frac{1}{z\mathbb{1} - M_{00} - \frac{M_{01} M_{01}^\dagger}{z\mathbb{1} - M_{11} - \tilde{\Sigma}_{11}(z)}} \quad (54)$$

where the self-energy matrix at the linear-linear level is

defined to be

$$\tilde{\Sigma}_{11}(z) = \frac{M_{12} M_{12}^\dagger}{z\mathbb{1} - M_{22} - \frac{M_{23} M_{32}^\dagger}{z\mathbb{1} - M_{33} - \dots}} \quad (55)$$

$$= \frac{M_{12} M_{12}^\dagger}{z\mathbb{1} - M_{22} - \tilde{\Sigma}_{22}(z)}. \quad (56)$$

For convenience a non-standard (but unique) notation for a matrix fraction has been introduced here, such that if A, B and C are matrices then

$$\frac{AB}{C} \equiv A \cdot C^{-1} \cdot B. \quad (57)$$

This notation saves a lot of space and avoids many nested parentheses and inverses that would be required in more standard notation. We remark that Eq. (52) is similar to the matrix formalism of Wu and Cao¹⁴, while Eq. (53) has similarities to the continued fraction formalisms of Mori^{47,48} and Schneider⁴⁹. The structure of Eq. (52) is that of a mode-coupling theory in which the role of mode order is played by the number of domains. The effect of the higher order modes is to renormalize the ‘‘transport’’ coefficients approximated by M^E at the linear level.

By truncating Eq. (53) at ever deeper levels, i.e., setting $M_{\alpha,\alpha+1} = 0$, corresponding to $\tilde{\Sigma}_{\alpha\alpha}(z) = 0$, for increasing α one gets expressions which work well for ever lower values of c , denoted as $\tilde{C}^{(\alpha)}(z)$. For example, truncating at the zeroth level gives

$$\tilde{C}^{(0)}(z) = \frac{1}{z - M_{00}} = \frac{1}{z + c}, \quad (58)$$

while truncating at the first, linear, level yields the result in Eq. (44). Following this procedure further, the first correction to the linear basis results involves evaluating the self-energy in the approximation where one ignores the effects of three-domains and higher, i.e. [cf. Eq (56)],

$$\tilde{\Sigma}_{11}(z) \approx \frac{M_{12} M_{12}^\dagger}{z\mathbb{1} - M_{22}}, \quad (59)$$

corresponding to a bi-linear type of mode-coupling theory. Due to the simplicity of the coupling with respect to mode order and for different domain sizes, an exact expression for this approximate self-energy can be obtained. In the appendix $\tilde{\Sigma}_{11}(z)$ is explicitly evaluated to be:

$$\tilde{\Sigma}_{11} = \begin{bmatrix} \tilde{\eta}_1 & -\sqrt{1-c}\tilde{\eta}_1 & & & \\ -\sqrt{1-c}\tilde{\eta}_1 & (1-c)\tilde{\eta}_1 + \tilde{\eta}_2 & -\sqrt{1-c}\tilde{\eta}_2 & & \\ & -\sqrt{1-c}\tilde{\eta}_2 & (2-c)\tilde{\eta}_2 & \ddots & \\ & & & \ddots & \ddots \end{bmatrix} \quad (60)$$

where the functions $\tilde{\eta}_j$ are given by Eqs. (A.21) and (A.25). Using this expression for the self-energy, the

linear-linear matrix $\tilde{\mathbf{G}}(z)$ of the previous section (which is in fact the top-left block of the inverse matrix on the

right hand side of Eq. (52) incorporating the zeroth and first level) is renormalized to

$$\tilde{\mathbf{G}}_R^{(2)} = \left[z\mathbb{1} - \mathbf{M}^E - \begin{pmatrix} 0 & 0 \\ 0 & \tilde{\Sigma}_{11} \end{pmatrix} \right]^{-1} \quad (61)$$

$$= \begin{bmatrix} z+c & \sqrt{c(1-c)} & & & & & & \\ \sqrt{c(1-c)} & z+1-\tilde{\eta}_1 & & & & & & \\ & -\sqrt{1-c}(c-\tilde{\eta}_1) & z+(2-c)(c-\tilde{\eta}_2) + (1-c)(\tilde{\eta}_2-\tilde{\eta}_1) & & & & & \\ & & -\sqrt{1-c}(c-\tilde{\eta}_2) & z+(2-c)(c-\tilde{\eta}_2) & & & & \\ & & & & \ddots & & & \\ & & & & & \ddots & & \\ & & & & & & \ddots & \\ & & & & & & & \ddots \end{bmatrix}^{-1} \quad (62)$$

from which the single spin time correlation function $\tilde{C}^{(2)} = [\tilde{\mathbf{G}}_R^{(2)}]_{11}$ is computed with the continued fraction expression in Eq. (39) to be

$$\tilde{C}^{(2)} = \frac{1}{z+c - \frac{c(1-c)}{\alpha(c,z)}} \quad (63)$$

where $\alpha(c,z)$ is

$$\alpha(c,z) = z+1-\tilde{\eta}_1 - \frac{(1-c)(c-\tilde{\eta}_1)^2}{z+(2-c)(c-\tilde{\eta}_2) + (1-c)(\tilde{\eta}_2-\tilde{\eta}_1) - \tilde{\gamma}^{(2)}}. \quad (64)$$

In Eq. (64), the repetitive part $\tilde{\gamma}^{(2)}$ satisfies

$$\tilde{\gamma}^{(2)} = \frac{(1-c)(c-\tilde{\eta}_2)^2}{z+(2-c)(c-\tilde{\eta}_2) - \tilde{\gamma}^{(2)}}. \quad (65)$$

This is solved by

$$\tilde{\gamma}^{(2)} = \frac{1}{2} \left\{ z+(2-c)(c-\tilde{\eta}_2) - \sqrt{4(c-\tilde{\eta}_2)z + (z-c(c-\tilde{\eta}_2))^2} \right\}. \quad (66)$$

Note the resemblance with $\tilde{\gamma}^{(1)}$ in Eq. (43).

As before, the exact result in Eq. (63) is inverted numerically using Stehfest's algorithm^{43,44,45}. For various values of c , the results are shown in Fig. 2 and compared with data from simulations of the East model. Notice that there is a huge improvement over the results obtained using only the single domain basis $\{\tilde{Q}_0, \tilde{Q}_1\}$ in Fig. 1. There is now excellent agreement between the theory and the data for $c \geq 0.4$, and reasonable agreement up to $c \approx 0.3$. Furthermore, while the theoretical decay is still too fast for $c < 0.3$, the small time behavior is captured beautifully. In particular, the shoulder that appears in the simulations for low c is reproduced by the extended theory as well, something the single domain basis could not do.

In the low temperature region (small c), the long time behavior of the spin autocorrelation function pre-

dicted by the two-domain basis set is well-described by a stretched exponential $C(t) \sim \exp[-(t/\tau)^\beta]$ with a temperature independent stretching exponent of $\beta \approx 0.6$. Although it is encouraging that the stretched exponential time profile is indeed predicted by the theory, simulations indicate that in fact the stretching exponent β should have a weak temperature dependence⁵⁰, with β decreasing in value as the temperature decreases. The origin of this discrepancy between our theory and numerical simulation is not clear and is under investigation.

In principle, the effect of three down-spin domains (trilinear modes) can be included in the same spirit, i.e., by evaluating the self-energy at the two-domain level $\tilde{\Sigma}_{22}(z)$ using matrix methods similar to those applied to obtain Eq. (60). Unfortunately, the algebra becomes even more cumbersome and explicit evaluation of the self-energy

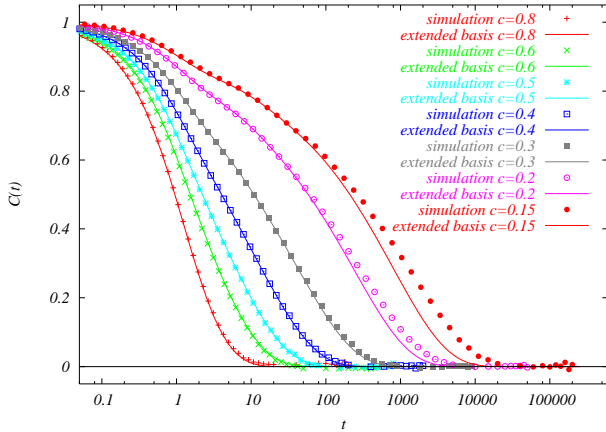


FIG. 2: Results for the single spin time correlation function $C(t)$ using the extended basis $\{\hat{Q}_0, \hat{Q}_1, \hat{Q}_2\}$ in Eq. (63) of Sec. VB (numerically Laplace inverted using *Mathematica*), compared to simulation data.

matrices at higher and higher order becomes effectively impossible. Alternatively, one can resort to numerical approaches in which the maximum domain size k_m is fixed and all matrix inversions are carried out numerically. By monitoring convergence to a set level of precision, such a procedure provides a systematic and numerically tractable method of predicting the decay of the spin autocorrelation function for arbitrary values of c .

VI. RELAXATION BEHAVIOR

One of the main advantages of the matrix method outlined here is that it is straightforward to obtain analytic predictions for rather detailed features of the dynamics. For example, one of the commonly calculated quantities from simulation data is the relaxation time τ . For systems exhibiting such non-trivial relaxation behavior as stretched-exponential, the definition of the relaxation time is a matter of choice. Perhaps the most sensible way to view the relaxation time for such systems is to consider it as the weighted-average of a distribution of relaxation times. For example, based on the spectral decomposition of the Liouville operator, one can formally write the spin autocorrelation function as a weighted sum of exponentials with relaxation times τ_n ,

$$C(t) = \sum_n c_n \exp(-t/\tau_n). \quad (67)$$

Since the Liouville operator is Hermitian and the spin variables are real, one is guaranteed that the relaxation times τ_n and coefficients $c_n = \langle \hat{Q}_0 | \psi_n \rangle^2$, where $|\psi_n\rangle$ are the right (and left) eigenvectors of the Liouvillian \mathcal{L} , are real and positive. Furthermore, since $C(t=0) = 1 = \sum_n c_n$, the coefficients c_n are proper weights for the relaxation time τ_n . However, since \mathcal{L} is of infinite dimension, its spectrum can be (partially or completely) contin-

uous, so the more general expression to replace Eq. (67) is

$$C(t) = \int \rho(\tau') \exp(-t/\tau') d\tau', \quad (68)$$

where $\rho(\tau') \geq 0$, $\rho(\tau' < 0) = 0$ and $\int \rho(\tau') d\tau' = 1$. One can therefore define the *average* relaxation time as

$$\tau = \int \rho(\tau') \tau' d\tau'. \quad (69)$$

Noting that the Laplace transform $\tilde{C}(z)$ of Eq. (68) is

$$\tilde{C}(z) = \int \frac{\rho(\tau')}{z + 1/\tau'} d\tau', \quad (70)$$

we see that

$$\tau = \int \rho(\tau') \tau' d\tau' = \tilde{C}(z=0). \quad (71)$$

Note that in the case in which a single relaxation time τ^* dominates all others, one observes that $\tau \approx \tau^*$ since $\rho(\tau') \approx \delta(\tau' - \tau^*)$.

Note also that in taking the point $z = 0$, the expression is sensitive to long time behavior. This in contrast to e.g. the average rate $\int \rho(\tau') (1/\tau') d\tau'$ which by Eq. (68) is just $-(d/dt)C(t=0) = c$ and contains no information on the long time behavior.

Given the analytical results for the Laplace transform of the spin autocorrelation function in the one-domain [Eq. (44)] and two-domain representations [Eq. (63)] of the slow dynamics, explicit expressions for $\tau(c)$ can be obtained by setting $z = 0$ in the respective equations. For example, not including domains as in Eq. (58) gives $\tau^{(0)} = 1/c$, while in the one-domain basis, Eqs. (44) and (71) lead to the simple result

$$\tau^{(1)} = \frac{1 - c + c^2}{c^3}, \quad (72)$$

in which the average relaxation time diverges as c^{-3} as the concentration c approaches zero. Furthermore, in the two-domain representation, the average relaxation time is a complicated function of c . In the limit that $c \rightarrow 0$, we find that $\tau^{(2)} \sim c^{-4}$. In Fig. (3), the theoretical predictions of the average relaxation time in the one-domain and two-domain basis sets are compared with numerically-integrated simulation data. Note that as is evident from Figs. (1) and (2), the two-domain predictions significantly improve the one-domain results but still underestimate the relaxation time of the system at small values of c .

From the relationship between c and $\beta\mu$ in Eq. (2), it is clear that at low temperatures $c \sim \exp(-\beta\mu)$. Since the logarithm of the average relaxation time $\log(\tau)$ is proportional to $\log(1/c)$ for $\tau^{(0)}$, $\tau^{(1)}$ and $\tau^{(2)}$, a plot of $\log(\tau)$ versus $\beta\mu$ yields a straight line in the small c (low temperature) limit. Thus we can conclude that the

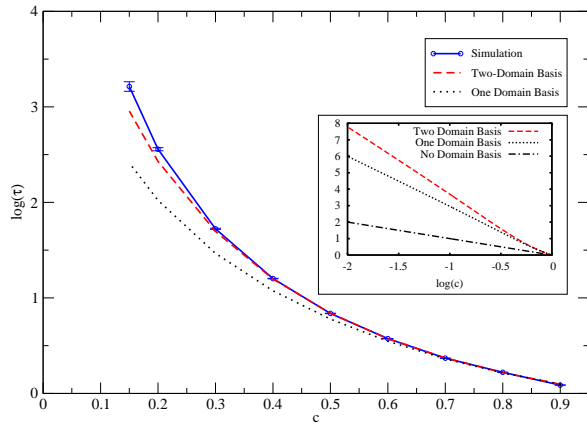


FIG. 3: Logarithm (base 10) of average relaxation time τ for various values of c . The inset shows the same as a function of the logarithm of c (also base 10) for the theoretical results, with slopes of -1 , -3 and -4 showing their scaling behavior.

zero, one and two-domain basis sets all yield a relaxation time that diverges according to the Vogel-Fulcher law $\tau \sim \exp\{-\text{const}/(T - T_0)\}$ with a glass transition temperature of $T_0 = 0$. Note that these results are in contrast with the exact result for the equilibration time τ_e of a system quenched to $T = 0$ where $\tau_e \sim \exp\{\text{const}/T^2\}$ ^{18,19}. This finding is somewhat surprising given that the equilibration time was calculated in the asymptotic small c regime using ideas of domain structure rather similar to those presented here.

Given the relatively simple structure of the matrix $\tilde{G}(z)$, it is easy to numerically examine many detailed features of the relaxation given a finite domain basis set specified by setting a maximum domain size k_m . For example, one can easily examine how the spectrum of \mathcal{L} depends on c . At the same time, the actual distribution of the c_n can be computed numerically to see how many relaxation modes are relevant as a function of c . From this information, one can try to attempt to establish a link between the distribution of relaxation times as a function of temperature and the asymptotic stretched exponential form, as suggested in reference¹⁵. This may be an instructive way to examine the failure of the two-domain basis to correctly predict the temperature dependence of the stretching exponent β . However since analytical results are available for all quantities, it is desirable to obtain analytical expressions for such features as the *width* or spread σ of the relaxation times τ' as a function of c . The spread in τ' is defined by

$$\sigma = \sqrt{\int \rho(\tau')(\tau' - \tau)^2 d\tau'}. \quad (73)$$

Now one can use that $\tilde{C}'(0) = \lim_{z \rightarrow 0} d/dz \tilde{C}(z) = -\int \rho(\tau')\tau'^2 d\tau'$ [cf. Eq. (71)] to write $\sigma = \{-\tilde{C}'(0) - [\tilde{C}(0)]^2\}^{1/2}$. Since we have obtained closed expressions for $\tilde{C}(z)$, analytic expressions can be ob-

tained for σ . For example, using the one-domain basis set, we find that

$$\sigma^{(1)} = \frac{\sqrt{1-c}}{c^3}, \quad (74)$$

whereas the expression for $\sigma^{(2)}$ in the two-domain basis is a complicated function of c [note: $\sigma^{(0)}$ is actually zero]. From these analytical expressions for σ , one immediately sees that, in fact, σ diverges as c approaches zero in the *same* way as τ . Hence a plot of σ/τ remains finite for all values of c . Furthermore, noting that in the one-domain basis,

$$\sigma^{(1)}/\tau^{(1)} = \frac{\sqrt{1-c}}{1-c+c^2}, \quad (75)$$

it is evident that $\lim_{c \rightarrow 0} \sigma^{(1)}/\tau^{(1)} = 1$. Surprisingly, the same conclusion holds in the two-domain basis, as is evident from Fig. 4. Note that at large values of $c \approx 1$, $\sigma \approx 0$ indicating that the relaxation is dominated by a single mode.

We note that higher order derivatives of $\tilde{C}(z)$ at $z = 0$ can similarly be used to investigate further characteristics of the relaxation time distribution such as the skewness and the kurtosis. More generally, Eq. (68) shows $C(t)$ to be the Laplace transform of the distribution of relaxation rates. If $r = 1/\tau$ are the relaxation rates, then their distribution is $P(r) = r^{-2}\rho(1/r)$ and Eq. (68) can be written as

$$C(t) = \int_0^\infty P(r) \exp(-rt) dr. \quad (76)$$

In this sense, $C(t)$ is the Laplace transform of $P(r)$. Thus, given $C(t)$, one might expect to be able to use the numerical Laplace inverse of the Stehfest algorithm to obtain $P(r)$. Unfortunately it turns out that using Stehfest's numerical Laplace inverse method on $C(t)$, which was itself obtained from $\tilde{C}(z)$ by the same method, is unstable; it in fact yields an incorrect result for $P(r)$, namely a highly oscillating function, which is not non-negative and not normalized to one. Since the distribution of relaxation rates was considered here mainly as an illustration of the power of the theoretical approach presented in this paper, solving the numerical instability associated with applying the Stehfest algorithm twice and determining the distribution of relaxation rates in detail, is left for future work.

VII. HIGHER ORDER CORRELATION FUNCTIONS

Given the glassy nature of the dynamics of the East model, it is interesting to probe higher order correlation functions to examine issues of cooperativity in the dynamics and non-Gaussian statistics. In particular, one

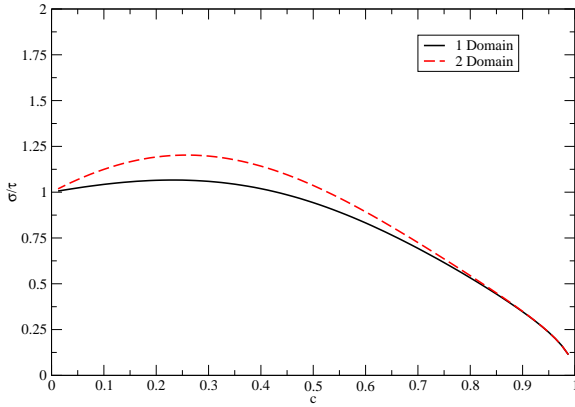


FIG. 4: Ratio σ/τ of the width σ of relaxation time distribution to the average relaxation time τ as a function of c , in the one-domain and two-domain bases.

can look at the neighbor-pair spin correlation function

$$\begin{aligned} \langle \hat{n}_i(t) \hat{n}_{i+1}(t) \hat{n}_i(0) \hat{n}_{i+1}(0) \rangle &= \langle \hat{Q}_1(k; t) \hat{Q}_1(k; 0) \rangle \delta_{k,0} \\ &= G_{22}(t), \end{aligned} \quad (77)$$

and a related quantity

$$\Delta(t) = G_{22}(t) - \langle \hat{n}_i(t) \hat{n}_i(0) \rangle \langle \hat{n}_{i+1}(t) \hat{n}_{i+1}(0) \rangle \quad (78)$$

that examines the non-Gaussian nature of the normalized spin fluctuation variable \hat{n}_i . Given the simplicity of the matrix method, it is relatively straightforward to obtain analytic expressions for higher order correlation functions such as Eq. (77). For example, from the definition of the neighbor-pair spin variable, which corresponds to the linear basis set element $\hat{Q}_1(0)$, it follows that the Laplace transform \tilde{G}_{22} of the function $G_{22}(t)$ is the $2-2$ element of the infinite matrix $\tilde{\mathbf{G}}$, which, in the two-domain basis approximation, is given by Eq. (61). Using standard matrix inversion methods, the $2-2$ element of $\tilde{\mathbf{G}}^{(2)}$ is

$$\tilde{G}_{22}^{(2)} = \frac{1}{\alpha(c, z) - \frac{c(1-c)}{z+c}}, \quad (79)$$

where $\alpha(c, z)$ is given in Eq. (64). In Fig. (5), the functions $G_{22}(t)$ and $\Delta(t)$ are plotted versus time for various values of c (using Stehfest’s algorithm for the inverse Laplace transform). Note that the agreement between the theoretical predictions and the simulation data is excellent for all times for all but the smallest value $c = 0.2$.

The neighbor-pair autocorrelation function exhibits several remarkable properties that are rather unlike those of the spin autocorrelation function. Note that in the short time limit $t \leq 1$ the relaxation of $G_{22}(t)$ is *independent* of the equilibrium up-spin concentration c . This result can be explained by examining a short time expansion (large z) of \tilde{G}_{22} , from which it is seen that

$\alpha(c, z) \sim z + 1$ and hence $\tilde{G}_{22} \sim 1/(z + 1)$, corresponding to simple exponential relaxation $G_{22}(t) \approx \exp(-t)$. Effectively this approximation corresponds to the short time expansion $\tilde{G}_{22} \sim 1/(z - \langle \hat{Q}_1(0) | \mathcal{L} | \hat{Q}_1(0) \rangle)$. Even more remarkable is the clear emergence of a plateau in the neighbor-pair autocorrelation function as c decreases and the system becomes “glassy”, yielding a two-step relaxation time profile similar to that observed for the dynamic structure factor at microscopic length scales in simple glass-forming systems. In such systems, the onset of the plateau, generally called the β -regime, is relatively insensitive to temperature and is often associated with the phenomenon of dynamic caging in dense fluid systems. In this regime, fluid particles typically oscillate in the traps formed by their immediate neighbors and little relaxation of the system occurs. This behavior typically continues until a typical time scale, known as the α -regime, is reached in which particle cages are temporarily broken. This α time scale is strongly temperature dependent and scales with the overall relaxation time of the system. Interestingly, similar behavior is observed in $G_{22}^{(2)}(t)$ of the East model: There is an initially rapid decay (with time scale $t \sim 1$) at which point a plateau appears. The plateau typically extends to times corresponding to the average relaxation time τ of the spin autocorrelation function. However, unlike simple liquid systems, the *height* of the plateau is strongly temperature dependent, occurring roughly at value of c . In the East model, one can interpret the emergence of the plateau as arising from a kind of effective dynamic caging of the pair spin variable $n_i n_{i+1}$ that occurs when $n_{i+1} = 1$. When the right neighbor of a given spin i is up, the spin n_i can oscillate between values of 1 and 0 for extended periods of time, corresponding to a kind of vibration in a cage. This behavior will persist until the spin $i + 1$ flips, which typically will occur at times $t \sim \tau$. Furthermore, the probability of finding such a caged system scales with the likelihood of finding an up-spin in equilibrium, c .

The two-step relaxation of $G_{22}(t)$ was also found numerically by Wu and Cao¹⁴ (who refer to this quantity C_2). Wu and Cao showed that the relaxation can be described with a stretched exponential behavior at long times. From the numerical analysis of our theoretical expressions, we find that the parameter-free *theoretical* relaxation profile is also well-described by a stretched exponential with the same stretching exponential $\beta \approx 0.6$ found in the analysis of the spin autocorrelation function $C(t)$.

As can be seen from Fig. (5), the spin fluctuations \hat{n}_i do not behave as Gaussian random variables at all time scales and for all values of c , unlike their counterpart, the Fourier components of the mass density, in simple liquid systems. It can also be observed that the decay of the spin fluctuations is slower than that predicted for a system exhibiting Gaussian statistics for all times at high values of c . As c drops below 0.5, the decay becomes *faster* than Gaussian at short times but slower than Gaussian at long times. The fact that $c = 0.5$ is

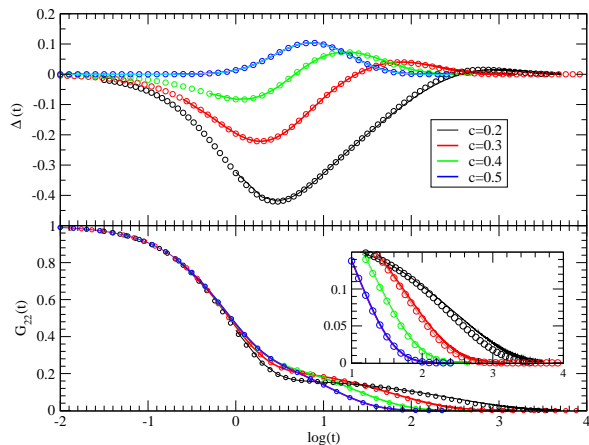


FIG. 5: Higher order correlation functions. Top: The non-Gaussian measure $\Delta(t)$ defined in Eq. (78). Bottom: The neighbor-pair auto-correlation function $G_{22}(t)$. In both graphs, open circles and solid lines correspond to *theoretical* and *simulation* values, respectively.

special can be seen from a short time expansion of $\Delta(t)$:

$$\begin{aligned} \Delta(t) &= \langle \hat{Q}_1(0) | e^{\mathcal{L}t} | \hat{Q}_1(0) \rangle - \langle \hat{Q}_0 | e^{\mathcal{L}t} | \hat{Q}_0 \rangle^2 \\ &= 1 + t \langle \hat{Q}_1(0) | \mathcal{L} | \hat{Q}_1(0) \rangle + \frac{t^2}{2} \langle \hat{Q}_1(0) | \mathcal{L}^2 | \hat{Q}_1(0) \rangle \\ &\quad - \left[1 + t \langle \hat{Q}_0 | \mathcal{L}^2 | \hat{Q}_0 \rangle + \frac{t^2}{2} \langle \hat{Q}_0 | \mathcal{L}^2 | \hat{Q}_0 \rangle \right]^2 + O(t^3). \end{aligned}$$

Using the rules elaborated in Sec. V A, all quantities appearing above are easily evaluated to reveal the exact result:

$$\Delta(t) = (2c - 1)t \left[1 - (2c + 1) \frac{t}{2} \right] + O(t^3), \quad (80)$$

from which the sign change for $c = 0.5$ is explicitly evident at short times.

One can also note in Fig. (5) that the maximum positive deviation from Gaussian behavior (i.e. slower than Gaussian) occurs at a time which scales roughly with the average relaxation time τ .

VIII. DISCUSSION

In this paper, the East model — a linear kinetically constrained spin model which is statically structureless — was studied theoretically taking the domains of down-spins as a starting point. The constraints in the model lead to a very slow spin relaxation for low up-spin density c because of the existence of these down-spin domains, of which each spin has to flip at least once before a spin on the left of the domain can relax. Such highly cooperative, hierarchical events driving the relaxation mimic heterogeneous behavior in glasses.

The way the down-spin domains were taken into account was by using them in the construction of a basis which is complete on the relevant ergodic component. In the complete domain basis, the theory is formally exact, but the basis needs to be truncated to get explicit results. In this truncation, one only limits how many simultaneous domains are included without restricting the possible sizes of those domains. When we restricted ourselves to a single domain description, an exact result for the single spin time correlation function $C(t)$ [$C^{(1)}$] was obtained which gives a good quantitative description for c larger than about 0.5. An extension including neighboring domains led to an exact expression [$C^{(2)}$] which described the slow, glassy behavior correctly down to $c \approx 0.3$. A general procedure was outlined to obtain further approximations.

The main advantages of our approach over others are that a) it gives explicit analytical results without fitting parameters, b) it requires neither an arbitrary closure for the memory kernel nor the construction of an irreducible memory kernel such as in mode coupling theories and c) nonetheless, it described low c behavior equally well as these mode coupling theories. The explanation for this power is that domains of all sizes are included.

At a given level of truncation, the matrix approach outlined here allows analytical results for the spin autocorrelation function to be obtained. Armed with these results, it is possible to assess the effect of truncation the multi-domain basis by evaluating approximate expressions for the “self-energy” terms, as was done in Sec. V. One can then examine the time scale at which the higher domain corrections become important and their magnitude for a given value of c . Such information is useful in examining dynamical scaling relations^{10,51}.

The matrix approach is also well-suited for examining higher-order correlation functions, such as the neighbor-pair auto-correlation function, that probe detailed aspects of the dynamics, as was shown in section VII.

Our theory does not require an ansatz for a closure relation between the memory kernel and the correlation function, yet it does have the *structure* of a mode coupling theory. First of all, the theory, derived using a projection operator formalism, yields a basis set very similar to the multi-linear set in the theory of Oppenheim *et al.* Secondly, successive truncations of the set are like including only linear modes, or also bilinear modes, or also tri-linear ones, etc., again very similar to mode coupling theories for fluids. Finally and perhaps most strikingly, without assuming a closure relation, a self-consistent equation emerges for part of the result, i.e., for $\tilde{\gamma}^{(1)}$ in Eq. (42) of Sec. V A and for $\tilde{\gamma}^{(2)}$ in Eq. (65) of Sec. V B. Thus, in a sense, the correct closure relation follows unambiguously from the theory rather than being assumed. Perhaps this is an indication why mode coupling theories can work, at least in some range of c , if the closure relation is well chosen. However, as the difference between the closure for $\tilde{\gamma}^{(1)}$ and $\tilde{\gamma}^{(2)}$ shows, the required closure depends on how low c is. The closure can also be

come ‘‘hierarchical’’, in the sense that $\tilde{\gamma}^{(2)}$ depends on $\tilde{\eta}_2$, which itself satisfies a self-consistent equation.

A natural question is how adaptable is the matrix approach outlined here for other conditions of spin facilitation, such as the Frederickson-Andersen^{6,7} (FA) model, higher-dimensions and other types of lattices. The extension to the FA model involves extending the one-domain basis set to include domains on *both* sides of the targeted spin and involves slightly more complicated matrix algebra than that presented here⁵². For the FA model for which self-consistent closure schemes in the context of mode-coupling theory appear to work quite well⁵³, quite good quantitative agreement can be obtained with the simple single-domain basis set. Extensions to include multiple domains can be carried out numerically for the FA model as well as other generic models. In addition, higher-dimensional models can also be tackled in a numerical fashion using finite basis set representations, provided the basis sets include domains that are sufficiently large. Although finite matrix representations are always bound to give the incorrect long time asymptotic behavior for systems exhibiting stretched-exponential profiles, the short and intermediate time behavior can be reproduced with great accuracy.

It is conceivable that the complete basis set presented in Sec. VB has a deeper structure that could be exploited for the description for $c \rightarrow 0$. Also, the domain basis might be used to describe the response of the East model to a sudden ‘‘quench’’ to low c values. Work on these issues is in progress.

Finally, our approach shows how important it is to *first* identify the ‘‘slow modes’’ of a system, in this case the down-spin domains, *before* embarking on a mode coupling-like description of the long time behavior of correlation functions.

Acknowledgments

This work was supported by a grant from the Natural Science and Engineering Research Council of Canada. For the final part of this project, R.V.Z. acknowledges the support of the Office of Basic Energy Sciences of the US Department of Energy, under grant No. DE-FG-02-88-ER13847. J.S. would also like to thank Walter Kob and the Laboratoire des Verres in Montpellier, France for their hospitality and the CNRS for additional funding during the final stages of this work.

APPENDIX: SELF-ENERGY MATRIX IN THE TWO-DOMAIN BASIS

From the expression for the self-energy matrix in the two-domain approximation,

$$\tilde{\Sigma}_{11}(z) \approx \frac{M_{12} M_{12}^\dagger}{z\mathbb{1} - M_{22}},$$

it is clear that we must evaluate matrices such as $M_{12} = \langle \hat{Q}_1(l) | \mathcal{L} | \hat{Q}_2(l_1, l_2) \rangle$. The double indices on $\hat{Q}_2(l_1, l_2)$ tend to make the algebra somewhat less transparent than in Sec. VA, and it turns out that the self-energy matrix can be evaluated more easily by splitting up the set \hat{Q}_2 into two-domain variables for which $l_2 = 0$ and those for which $l_2 > 0$, by defining

$$\hat{R}(k) = \hat{Q}_2(k, 0) \quad (\text{A.1})$$

$$\hat{S}(l_1, l_2) = \hat{Q}_2(l_1, l_2 + 1) \quad (\text{A.2})$$

and likewise for unnormalized versions, as indicated in Table III. The matrix M_{12} then takes on the form $M_{12} = [M_{QR}, M_{QS}]$, where

$$M_{QR} = \langle \hat{Q}_1 | \mathcal{L} | \hat{R} \rangle \quad (\text{A.3})$$

$$M_{QS} = \langle \hat{Q}_1 | \mathcal{L} | \hat{S} \rangle \quad (\text{A.4})$$

and M_{22} is written in the block form

$$M_{22} = \begin{bmatrix} M_{RR} & M_{RS} \\ M_{RS}^\dagger & M_{SS} \end{bmatrix} \quad (\text{A.5})$$

where M_{RR} , M_{RS} and M_{SS} are

$$M_{RR} = \langle \hat{R} | \mathcal{L} | \hat{R} \rangle \quad (\text{A.6})$$

$$M_{RS} = \langle \hat{R} | \mathcal{L} | \hat{S} \rangle \quad (\text{A.7})$$

$$M_{SS} = \langle \hat{S} | \mathcal{L} | \hat{S} \rangle, \quad (\text{A.8})$$

and where the notation that \hat{R} or \hat{S} without any argument denotes the column or row vector composed of all $\hat{R}(k)$ or $\hat{S}(k_1, k_2)$ respectively.

The matrix M_{QS} is in fact zero, so the matrix self-energy $\tilde{\Sigma}_{11}$ is

$$\tilde{\Sigma}_{11} = M_{QR} \left[z\mathbb{1} - M_{22} \right]_{RR}^{-1} M_{QR}^\dagger. \quad (\text{A.9})$$

Using the matrix equality (51), this expression can be re-written as

$$\begin{aligned} \tilde{\Sigma}_{11} &= M_{QR} \left[z\mathbb{1} - M_{RR} - \frac{M_{RS} M_{RS}^\dagger}{z\mathbb{1} - M_{SS}} \right]^{-1} M_{QR}^\dagger \\ &= \frac{M_{QR} M_{QR}^\dagger}{z\mathbb{1} - M_{RR} - \frac{M_{RS} M_{RS}^\dagger}{z\mathbb{1} - M_{SS}}}. \end{aligned} \quad (\text{A.10})$$

The explicit calculation of all the matrix elements appearing in Eq. (A.10) proceeds as follows: We start with M_{QR} defined in Eq. (A.3). Combining the diagrams of $\mathcal{L}Q_1(k)$ in Eqs. (32b) and (32c) with the diagrams of $R(k') = Q_2(k', 0)$ in Table III yields

$$\begin{aligned} \langle Q_1(k) | \mathcal{L} | R(k-1) \rangle &= (1-c) \textcircled{\scriptsize k-1} = c^3(1-c)^{k+3} \\ \langle Q_1(k) | \mathcal{L} | R(k) \rangle &= -\textcircled{\scriptsize k} = -c^3(1-c)^{k+3} \end{aligned}$$

while all other $\langle Q_1(k)|\mathcal{L}|R(k')\rangle$ are zero. By similar diagrammatic means, one finds $\langle S(l_1, l_2)|\mathcal{L}|Q_1(k)\rangle = 0$ — so that M_{QS} in Eq. (A.4) is indeed zero as we anticipated above. Also $\langle R(k)|\mathcal{L}|Q_0\rangle = \langle S(l_1, l_2)|\mathcal{L}|Q_0\rangle = 0$, confirming that $M_{02} = 0$. Using Eqs. (A.3), as well as (24) and (46) gives

$$M_{QR} = \begin{bmatrix} -(1-c)c^{1/2} & 0 & & \\ (1-c)^{3/2}c^{1/2} & \ddots & \ddots & \\ & & \ddots & \\ & & & \ddots \end{bmatrix}. \quad (\text{A.11})$$

Next we will determine M_{RR} defined in (A.6). For this we need the diagrams of $\mathcal{L}R(k)$:

$$\mathcal{L}R(0) = -\bullet\bullet\bullet - (1-c)\bullet\bullet\bullet - \bullet\bullet\bullet \quad (\text{A.12})$$

$$\mathcal{L}R(k \geq 1) = -\overset{k}{\circ}\text{---}\bullet\bullet - (1-c)\overset{k}{\circ}\text{---}\bullet\bullet + \overset{k-1}{\circ}\text{---}\bullet\bullet \quad (\text{A.13})$$

Combining these diagrams with those of $R(k')$ in Table III yields

$$\begin{aligned} \langle R(0)|\mathcal{L}|R(0)\rangle &= -\bullet\bullet\bullet - (1-c)\bullet\bullet\bullet - \bullet\bullet\bullet \\ &= -c^3(1-c)^2(2-c+c^2) \end{aligned} \quad (\text{A.14})$$

$$\begin{aligned} \langle R(k)|\mathcal{L}|R(k)\rangle &= -\overset{k}{\circ}\text{---}\bullet\bullet - (1-c)\overset{k}{\circ}\text{---}\bullet\bullet + \overset{k-1}{\circ}\text{---}\bullet\bullet \\ &= -c^3(1-c)^{k+2}(1+c^2) \text{ if } k \geq 1 \end{aligned} \quad (\text{A.15})$$

while $\langle R(k)|\mathcal{L}|R(k')\rangle = 0$ if $k \neq k'$. Using also Eqs. (46) and (47), one finds

$$[M_{RR}]_{kk'} = -(2-c+c^2)\delta_{k0}\delta_{kk'} - (1+c^2)(1-\delta_{k0})\delta_{kk'}, \quad (\text{A.16})$$

Next to determine is M_{RS} . Combining the diagrams of S in Table III with those of $\mathcal{L}R$ in Eqs. (A.12) and (A.13), we see that many elements of M_{RS} are zero, while the nonzero ones are restricted to

$$\langle S(k, 0)|\mathcal{L}|R(k)\rangle = -\overset{k}{\circ}\text{---}\bullet\bullet = c^4(1-c)^{k+3} \quad (\text{A.17})$$

for all $k \geq 0$. Using Eqs. (46) and (A.7), we find

$$[M_{RS}]_{kl_1l_2} = c(1-c)^{1/2}\delta_{l_1k}\delta_{l_20} \quad (\text{A.18})$$

The final matrix to determine is M_{SS} , for which we require $\mathcal{L}S(l_1, l_2)$:

$$\begin{aligned} \mathcal{L}S(0, l_2) &= -\overset{l_2+1}{\circ}\text{---}\bullet + (1-c)\overset{l_2}{\circ}\text{---}\bullet\bullet - \overset{l_2+1}{\circ}\text{---}\bullet\bullet \\ \mathcal{L}S(l_1 \geq 1, l_2) &= \overset{l_1-1}{\circ}\text{---}\overset{l_2+1}{\circ}\text{---}\bullet + (1-c)\overset{l_1}{\circ}\text{---}\overset{l_2}{\circ}\text{---}\bullet \\ &\quad - \overset{l_1}{\circ}\text{---}\overset{l_2+1}{\circ}\text{---}\bullet. \end{aligned}$$

Combining with the diagrams of S in Table III, one finds

$$\begin{aligned} \langle S(0, l_2)|\mathcal{L}|S(0, l_2)\rangle &= -(1+2c-c^2)c^3(1-c)^{3+l_2} \\ \langle S(0, l_2+1)|\mathcal{L}|S(0, l_2)\rangle &= c^4(1-c)^{l_2+4} \\ \langle S(l_1 \geq 1, l_2)|\mathcal{L}|S(l_1, l_2)\rangle &= -(3-c)c^4(1-c)^{l_1+l_2+3} \\ \langle S(l_1 \geq 1, l_2+1)|\mathcal{L}|S(l_1, l_2)\rangle &= c^4(1-c)^{l_1+l_2+4}, \end{aligned}$$

while all other $\langle S|\mathcal{L}|S\rangle$ are zero. Combining with Eqs. (46) and (A.8), one gets

$$\begin{aligned} [M_{SS}]_{l_1l_2l'_1l'_2} &= \delta_{l_1l'_1}[(\delta_{l'_2l_2+1} + \delta_{l'_2l_2-1})c(1-c)^{1/2} \\ &\quad - \delta_{l'_2l_2}\delta_{l_10}(1+2c-c^2) \\ &\quad - \delta_{l'_2l_2}(1-\delta_{l_10})c(3-c)]. \end{aligned} \quad (\text{A.19})$$

In view of Eqs. (A.10) and (A.18), we need the $l_2 = 0, l'_2 = 0$ component of the inverse of $z\mathbb{1} - M_{SS}$. This matrix is diagonal in l_1 and l'_1 and tri-diagonal in l_2 and l'_2 for fixed l_1 and l'_1 . Thus, we can use Eq. (39) to write

$$[z\mathbb{1} - M_{SS}]_{l_1,0;l_1,0}^{-1} = \frac{\delta_{l_10}}{\tilde{a}_1 - \tilde{\varepsilon}_1} + \frac{1 - \delta_{l_10}}{\tilde{a}_2 - \tilde{\varepsilon}_2}, \quad (\text{A.20})$$

where

$$\tilde{a}_1 = z + 1 + 2c - c^2 \quad (\text{A.21a})$$

$$\tilde{a}_2 = z + c(3-c). \quad (\text{A.21b})$$

and $\tilde{\varepsilon}_1$ and $\tilde{\varepsilon}_2$ result from the repeating part of the continued fraction that results from applying Eq. (39). Similar to $\tilde{\gamma}^{(1)}$ in Eq. (42) in section V A, they satisfy

$$\tilde{\varepsilon}_j = c^2(1-c)/(\tilde{a}_j - \tilde{\varepsilon}_j). \quad (\text{A.22})$$

With the requirement that they go as $1/z$ for large z , the solutions are

$$\tilde{\varepsilon}_j = \frac{1}{2} \left[\tilde{a}_j - \sqrt{\tilde{a}_j^2 - 4c^2(1-c)} \right]. \quad (\text{A.23})$$

The subexpression $M_{RS}[z\mathbb{1} - M_{SS}]^{-1}M_{RS}^\dagger$ in Eq. (A.10) now becomes, using Eq. (A.18), (A.20), (A.21) and (A.22)

$$\left[\frac{M_{RS}M_{RS}^\dagger}{z\mathbb{1} - M_{SS}} \right]_{kk'} = \delta_{kk'} [\tilde{\varepsilon}_1\delta_{k0} + \tilde{\varepsilon}_2(1-\delta_{k0})] \quad (\text{A.24})$$

Since this matrix and M_{SS} in Eq. (A.16) are diagonal, the inverse of $(z\mathbb{1} - M_{RR} - M_{RS}[z\mathbb{1} - M_{SS}]^{-1}M_{RS}^\dagger)$ is simply

$$\begin{aligned} &\left[z\mathbb{1} - M_{RR} - \frac{M_{RS}M_{RS}^\dagger}{z\mathbb{1} - M_{SS}} \right]_{kk'}^{-1} \\ &= \frac{\delta_{k0}\delta_{kk'}}{z + 2 - c + c^2 - \tilde{\varepsilon}_1} + \frac{(1-\delta_{k0})\delta_{kk'}}{z + 1 + c^2 - \tilde{\varepsilon}_2} \\ &= \frac{\delta_{kk'}}{1-c} \left[\frac{\delta_{k0}}{1-2c+c^2/\tilde{\varepsilon}_1} + \frac{1-\delta_{k0}}{1-2c+c^2/\tilde{\varepsilon}_2} \right], \end{aligned}$$

where in the last equality we used again Eq. (A.22). Given this last form, we can shorten many equations by using the expressions $\tilde{\eta}_j = c(1-c)/(1-2c+c^2/\tilde{\varepsilon}_j)$, which are explicitly given by

$$\tilde{\eta}_j = \frac{c(1-c)}{1-2c + \frac{2c^2}{\tilde{a}_j - \sqrt{\tilde{a}_j^2 - 4c^2(1-c)}}}. \quad (\text{A.25})$$

and in terms of which we have

$$\left[z\mathbb{1} - M_{RR} - \frac{M_{RS} M_{RS}^\dagger}{z\mathbb{1} - M_{SS}} \right]_{kk'}^{-1} = \frac{\delta_{kk'} [\tilde{\eta}_1 \delta_{k0} + \tilde{\eta}_2 (1 - \delta_{k0})]}{c(1-c)^2}.$$

Inserting this result in the expression for the self-energy matrix in Eq. (A.10), one obtains the result presented in Eq. (60).

- ¹ C. A. Angell, *Science* **267**, 1924 (1995).
- ² M. D. Ediger, C. A. Angell, and S. R. Nagel, *J. Phys. Chem.* **100**, 13200 (1996).
- ³ P. G. Debenedetti and F. H. Stillinger, *Nature* **410**, 259 (2001).
- ⁴ M. D. Ediger, *Annu. Rev. Phys. Chem.* **51**, 99 (2000).
- ⁵ J. Jäckle and S. Eisinger, *Z. Phys. B: Condens. Mat.* **84**, 115 (1991).
- ⁶ G. H. Frederickson and H. C. Andersen, *Phys. Rev. Lett.* **53**, 1244 (1984).
- ⁷ G. H. Frederickson and H. C. Andersen, *J. Chem. Phys.* **83**, 5822 (1985).
- ⁸ S. J. Pitts, T. Young, and H. C. Andersen, *J. Chem. Phys.* **113**, 8671 (2000).
- ⁹ S. J. Pitts and H. C. Andersen, *J. Chem. Phys.* **114**, 1101 (2001).
- ¹⁰ F. Ritort and P. Sollich, *Adv. Phys.* **52**, 219 (2003).
- ¹¹ J. P. Garrahan and D. Chandler, *Phys. Rev. Lett.* **89**, 035704 (2002).
- ¹² J. P. Garrahan and D. Chandler, *Proc. Natl. Acad. Sci. USA* **100**, 9710 (2003).
- ¹³ P. Sollich and M. R. Evans, *Phys. Rev. E* **68**, 031504 (2003).
- ¹⁴ J. Wu and J. Cao, *J. Chem. Phys. B* **108**, 6796 (2004).
- ¹⁵ R. G. Palmer, D. L. Stein, E. Abrahams, and P. W. Anderson, *Phys. Rev. Lett.* **53**, 958 (1984).
- ¹⁶ W. Götze and L. Sjögren, *J. Phys. C: Solid State Phys.* **21**, 3407 (1998).
- ¹⁷ J. C. Phillips, *Rep. Prog. Phys.* **55**, 241 (1996).
- ¹⁸ P. Sollich and M. R. Evans, *Phys. Rev. Lett.* **83**, 3238 (1999).
- ¹⁹ D. Aldous and P. Diaconis, *J. Stat. Phys.* **107**, 945 (2002).
- ²⁰ W. Götze and M. Lücke, *Phys. Rev. A* **11**, 2173 (1975).
- ²¹ J. Bosse, W. Götze, and M. Lücke, *Phys. Rev. A* **17**, 434 (1978).
- ²² U. Bengtzelius, W. Götze, and A. Sjölander, *J. Phys. C* **17**, 5915 (1984).
- ²³ E. Leutheusser, *Phys. Rev. A* **29**, 2765 (1984).
- ²⁴ W. Götze and L. Sjögren, *Z. Phys. B: Condens. Mat.* **65**, 415 (1987).
- ²⁵ M. Fuchs, W. Götze, I. Hofacker, and A. Latz, *J. Phys.: Condens. Matter* **3**, 5047 (1991).
- ²⁶ W. Götze and L. Sjögren, *Rep. Prog. Phys.* **55**, 241 (1992).
- ²⁷ H. Z. Cummins, W. M. Du, M. Fuchs, W. Götze, S. Hildebrand, and A. Latz, *Phys. Rev. E* **47**, 4223 (1993).
- ²⁸ M. Fuchs, W. Götze, and M. R. Mayr, *Phys. Rev. E* **58**, 3384 (1998).
- ²⁹ W. Götze, *J. Phys.: Condens. Matter* **11**, A1 (1999).
- ³⁰ W. Götze and M. Sperl, *Phys. Rev. E* **66**, 011405 (2002).
- ³¹ J. Machta and I. Oppenheim, *Physica* **112A**, 361 (1982).
- ³² J. Schofield, R. Lim, and I. Oppenheim, *Physica* **181A**, 89 (1992).
- ³³ C. Z.-W. Liu and I. Oppenheim, *Physica A* **235**, 369 (1997).
- ³⁴ C. Z.-W. Liu and I. Oppenheim, *Physica A* **247**, 183 (1997).
- ³⁵ H. C. Andersen, *J. Phys. Chem. B* **106**, 8326 (2002); **107**, 10226; **107** 10234 (2003).
- ³⁶ K. Kawasaki, *Physica* **215A**, 61 (1995).
- ³⁷ N. G. van Kampen, *Stochastic Processes in Physics and Chemistry* (North Holland, Amsterdam, 1992), revised and enlarged ed.
- ³⁸ T. Keyes, in *Statistical Mechanics, Part B*, edited by B. J. Berne (Plenum Press, New York, 1977).
- ³⁹ R. Zwanzig, *Nonequilibrium Statistical Mechanics* (Oxford University Press, New York, 2001).
- ⁴⁰ H. Mori, *Phys. Rev.* **112**, 1829 (1958).
- ⁴¹ P. Kavassalis and I. Oppenheim, *Physica* **148A**, 521 (1988).
- ⁴² S. J. Pitts and H. C. Andersen, *J. Chem. Phys.* **113**, 3945 (2000).
- ⁴³ H. Stehfest, *Comm. ACM* **13**, 47 (1970).
- ⁴⁴ H. Stehfest, *Comm. ACM* **13**, 624 (1970).
- ⁴⁵ A. Mallet, *Numerical inversion of Laplace transform* (2000). These packages for *Mathematica* can be downloaded from <http://library.wolfram.com/infocenter/MathSource/2691/>.
- ⁴⁶ W. H. Press, S. A. Teukolsky, W. T. Vetterling, and B. P. Flannery, *Numerical Recipes in Fortran, The Art of Scientific Computing* (Cambridge University Press, 1992), 2nd ed.
- ⁴⁷ H. Mori, *Prog. Theor. Phys.* **33**, 423 (1965).
- ⁴⁸ H. Mori, *Prog. Theor. Phys.* **34**, 399 (1965).
- ⁴⁹ W. R. Schneider, *Z. Phys. B: Condens. Mat.* **24**, 135 (1976).
- ⁵⁰ L. Berthier and J. P. Garrahan, *J. Chem. Phys.* **119**, 4367 (2003).
- ⁵¹ S. Whitelam, L. Berthier, and J. P. Garrahan, *Phys. Rev. Lett.* **92**, 185705 (2004).
- ⁵² R. van Zon and J. Schofield, unpublished.
- ⁵³ G. Szamel, *J. Chem. Phys.* **121**, 3355 (2004).